Time-dependent embedding

2008 J. Phys.: Condens. Matter 20 095215

(http://iopscience.iop.org/0953-8984/20/9/095215)

J. Phys.: Condens. Matter **20** (2008) 095215 (13pp) doi:10.1088/0953-8984/20/9/095215

Time-dependent embedding

J E Inglesfield

School of Physics and Astronomy, Cardiff University, Cardiff CF24 3YB, UK

Received 14 December 2007
Published 14 February 2008
Online at stacks.iop.org/JPhysCM/20/095215

Abstract

A method of solving the time-dependent Schrödinger equation is presented, in which a finite region of space is treated explicitly, with the boundary conditions for matching the wavefunctions to the rest of space replaced by an embedding term added on to the Hamiltonian. This time-dependent embedding term is derived from the Fourier transform of the energy-dependent embedding potential, which embeds the time-independent Schrödinger equation. Results are presented for a one-dimensional model of an atom in a time-varying electric field, the surface excitation of this model atom at a jellium surface in an external electric field, and the surface excitation of a bulk state.

1. Introduction

The availability of ultra-short laser pulses [1] opens up new ways of studying time-dependent electronic processes in atoms [2, 3], molecules [4] and at solid surfaces [5]. In surface physics the time delay of a core electron emitted through the surface potential barrier can now be compared on an attosecond timescale with valence electron photoemission in time-resolved photoemission experiments [6]. This makes it important to develop appropriate theoretical tools for studying such processes, in particular for solving the time-dependent Schrödinger equation accurately. A problem arises with the boundary in solving this equation—if an electron is ejected from an atom, for example, how is its wavefunction treated as it propagates outwards towards the edge of the computational region? One approach is to apply absorbing boundary conditions at the edge of the region [7], but this is an approximation [8]; complex coordinate methods can also be used to remove the outgoing wave in solutions of the time-dependent Schrödinger equation [9]. Other methods are used in atomic physics to study photo-ionization in particular—the wavefunction can be expanded in complex basis functions [10], and Floquet methods use a Floquet–Fourier series expansion of the wavefunction [11].

In recent years there has been work on transparent boundary conditions, so that the solution of the time-dependent Schrödinger equation in some restricted region of interest, which we call region I, propagates out through the boundary into the rest of the system, region II, without reflection. It has been shown by Hellums and Frensley [12] using a matrix partitioning of the Hamiltonian that these boundary conditions are equivalent to an extra 'memory' term—a time-dependent embedding or self-energy term—added to the Hamiltonian. This spatial partitioning, and the corresponding form of the embedding term, is appropriate for a Hamiltonian constructed with localized basis functions or spatially discretized wavefunctions.

An embedding method for solving the time-independent Schrödinger equation in the region of interest was developed many years ago by the author [13, 14]. The operator which embeds region I—the embedding potential—is given by the surface inverse of a Green function for region II, evaluated over the boundary between the regions. Any convenient basis set can be used to expand the wavefunctions (or Green function) in region I, and the method has been widely used in accurate surface calculations [15], and recently in photonics applications [16]. The embedding potential is a generalized logarithmic derivative, giving the normal derivative of the wavefunction over the boundary of region I in terms of the amplitude—in mathematical terms it is a Dirichlet-to-Neumann map [17]. It is this form of embedding potential, rather than a tight-binding or discretized form, which we shall apply in this paper to the time-dependent problem.

The time-dependent version of the Dirichlet-to-Neumann map has been studied by Ehrhardt [18], and applied to embedding the time-dependent Schrödinger equation, discretized spatially as well as temporally—Ehrhardt paid particular attention to the stability and accuracy of the time evolution. Moyer [19] has used this to study a range of one-dimensional problems including the scattering of electrons in model semiconductor structures. Recently, Kurth *et al* [20] have developed a spatially discretized method to study quantum transport through a structure between two leads, replacing the leads by time-dependent embedding self-energies; they also consider time-varying bias potentials in the leads. Boucke *et al* [8] have applied the time-dependent relationship between normal derivative and amplitude to the one-dimensional problem of an oscillating potential of the

form $V(z,t) = -1/\cosh^2[z + \xi_0 \sin(\omega t)]$ acting on the wavefunction $1/\cosh(z)$. (This wavefunction is the bound state of the static potential; the oscillating potential is equivalent, by the Kramers–Henneberger transformation [21], to the static potential in a spatially uniform time-varying electric field.) They solve this problem on a finite spatial grid, with the boundary relationship, for zero potential in the external region, applied to the end grid points.

Instead of using a finite-difference grid, Ermolaev *et al* [22] expand the wavefunction in region I in a basis set. The matrix element of the kinetic energy operator evaluated over this finite region of space gives a normal derivative term at the boundary of region I, and this is evaluated using the Green function relationship with the boundary amplitude. They also consider the time evolution of the bound state of the $-1/\cosh^2(z)$ potential, but instead of transforming the spatially homogeneous, time-varying electric field using the Kramers–Henneberger transformation, they treat the problem directly, with a sinusoidally varying field in region II. Like Ermolaev *et al*, we will also use a basis set for expanding the wavefunction in region I, but we incorporate the amplitude–derivative relationship in a way analogous to the energy-dependent embedding method [13].

We begin this paper with a derivation in section 2 of the time-dependent embedding method, based on our original method for embedding the stationary Schrödinger equation. In section 3 we derive the time-dependent embedding potential analytically for a constant external potential in region II, and demonstrate a numerical technique for embedding on to a constant electric field. We move on to model applications in sections 4 and 5. In section 4 we shall consider the same problem as Boucke *et al* [8]—the oscillating potential $-1/\cosh^2[z + \xi_0 \sin(\omega t)]$ acting on the $1/\cosh z$ bound state, using a very small region I enclosing this potential and embedding on to zero potential on either side. We shall see that the results are in excellent agreement with a finite-difference calculation extending a large distance on either side of the time-varying potential. In this section we shall next consider the excitation of a localized wavefunction at the surface of a free-electron metal by a time-dependent perturbation, with a static electric field on the vacuum side of the surface. We could use this in a model of photo-assisted field emission [23], or even pump–probe experiments; here the calculation provides a test of the embedding potential for a uniform electric field.

The problems that we solve in section 4 are restricted to wavefunctions confined initially to region I, though in the course of time evolution they leak outside. This is a severe restriction for surface physics or other condensed matter applications, where the initial wavefunction is usually an extended state. In section 5 we shall show how the time evolution of such wavefunctions can be calculated using embedding, with region I containing the time-dependent perturbing potential, but not necessarily the starting wavefunction. The model calculation that we shall describe in section 5 corresponds to the surface of a free-electron metal, with a sinusoidal time-dependent potential applied in the surface region (region I). With a small basis set, the time evolution of the bulk wavefunctions at the surface can be calculated very accurately.

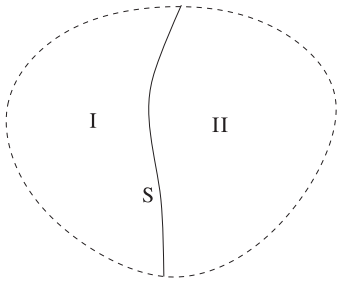

Figure 1. Region I is embedded on to region II over surface S.

Atomic units are used throughout this paper, with $e = \hbar = m_e = 1$. The atomic unit of time $= 2.418\,884 \times 10^{-17}$ s, so that 1 fs $= 41.341\,38$ au.

2. Stationary and time-dependent embedding

In this section we shall start from our previous results for embedding the stationary Schrödinger equation [13], and show how these can be transformed into time-dependent embedding. The embedding problem can be represented schematically by figure 1. We wish to solve the Schrödinger equation—either time-independent or time-dependent—in the whole system, regions I + II: region I is treated explicitly, and region II is replaced by an 'embedding potential' at the interface S, added on to the Hamiltonian for region I. In a typical application to surfaces, region I would be the surface layer or two of atoms together with the potential barrier region, and region II would be the vacuum on one side and the substrate crystal on the other [15]. The embedding potential ensures that the wavefunctions evaluated in region I match correctly in amplitude and derivative on to the appropriate solutions of the Schrödinger equation in region II.

2.1. Stationary embedding

The original embedding method is based on a variational principle for the energy, and here we shall outline the derivation [13, 14]. The one-electron Hamiltonian, of which we wish to find the expectation value, is given by

$$H = -\tfrac{1}{2}\nabla^2 + V(\mathbf{r}), \tag{1}$$

where V is the one-electron potential. In region I we have an arbitrary trial function ϕ; this is extended through region II with the exact solution ψ of the Schrödinger equation, evaluated at some trial energy ϵ, which matches in amplitude on to ϕ over the boundary S joining the regions (figure 1). It is assumed that at an external boundary (the dashed line in figure 1), the wavefunctions satisfy a homogeneous boundary condition, typically going to zero. The expectation value of H is then given by

$$E = \frac{\int_{\mathrm{I}} \mathrm{d}\mathbf{r}\, \phi^* H \phi + \epsilon \int_{\mathrm{II}} \mathrm{d}\mathbf{r}\, \psi^* \psi + \frac{1}{2}\int_{\mathrm{S}} \mathrm{d}\mathbf{r}_{\mathrm{S}}\, \phi^* \left(\frac{\partial \phi}{\partial n_{\mathrm{S}}} - \frac{\partial \psi}{\partial n_{\mathrm{S}}}\right)}{\int_{\mathrm{I}} \mathrm{d}\mathbf{r}\, \phi^* \phi + \int_{\mathrm{II}} \mathrm{d}\mathbf{r}\, \psi^* \psi}. \tag{2}$$

The first two terms in the numerator are the expectation values of the Hamiltonian in regions I and II. The third term, an integral over the boundary S, contains the difference in normal derivatives on either side of S (measured outwards from I) and comes from the kinetic energy operator acting on the kink in the trial function.

We now use a result obtained by applying Green's theorem in region II,

$$\psi(\mathbf{r}_S) = -\frac{1}{2}\int_S \mathrm{d}\mathbf{r}'_S\, G_0(\mathbf{r}_S, \mathbf{r}'_S; \epsilon)\frac{\partial\psi(\mathbf{r}'_S)}{\partial n_S}. \tag{3}$$

G_0 is the Green function in II satisfying the zero normal derivative boundary condition on S. Taking the inverse of (3) gives the result which is central to the embedding method,

$$\frac{\partial\psi(\mathbf{r}_S)}{\partial n_S} = -2\int_S \mathrm{d}\mathbf{r}'_S G_0^{-1}(\mathbf{r}_S, \mathbf{r}'_S; \epsilon)\psi(\mathbf{r}'_S), \tag{4}$$

where G_0^{-1} is the surface inverse over S. G_0^{-1} is the embedding potential and, as we see from equation (4), it is a generalized logarithmic derivative. G_0^{-1} is the same as the mathematicians' Dirichlet-to-Neumann map [17, 24], mapping the Dirichlet boundary condition (the amplitude specified over the boundary) on to the Neumann (the derivative specified). Using this result, and the fact that $\psi = \phi$ over the boundary, we obtain

$$\int_S \mathrm{d}\mathbf{r}\,\phi^*\frac{\partial\psi}{\partial n_S} = -2\int_S \mathrm{d}\mathbf{r}_S\int_S \mathrm{d}\mathbf{r}'_S\,\phi^*(\mathbf{r}_S)G_0^{-1}(\mathbf{r}_S, \mathbf{r}'_S; \epsilon)\phi(\mathbf{r}'_S). \tag{5}$$

To complete the simplification of equation (2), we use a second result involving the embedding potential [13],

$$\int_{\mathrm{II}} \mathrm{d}\mathbf{r}\,\psi^*\psi = -\int_S \mathrm{d}\mathbf{r}_S\int_S \mathrm{d}\mathbf{r}'_S\,\phi^*(\mathbf{r}_S)\frac{\partial G_0^{-1}(\mathbf{r}_S, \mathbf{r}'_S; \epsilon)}{\partial\epsilon}\phi(\mathbf{r}'_S). \tag{6}$$

Substituting (5) and (6) into (2) gives us the embedding variational principle,

$$\begin{aligned} E = &\left\{\int_I \mathrm{d}\mathbf{r}\,\phi^* H\phi + \frac{1}{2}\int_S \mathrm{d}\mathbf{r}_S\phi^*\frac{\partial\phi}{\partial n_S}\right. \\ &+ \left.\int_S \mathrm{d}\mathbf{r}_S\int_S \mathrm{d}\mathbf{r}'_S\phi^*\left(G_0^{-1} - \epsilon\frac{\partial G_0^{-1}}{\partial\epsilon}\right)\phi\right\} \\ &\times\left\{\int_I \mathrm{d}\mathbf{r}\,\phi^*\phi - \int_S \mathrm{d}\mathbf{r}_S\int_S \mathrm{d}\mathbf{r}'_S\,\phi^*\frac{\partial G_0^{-1}}{\partial\epsilon}\phi\right\}^{-1}. \end{aligned} \tag{7}$$

This gives E in terms of the trial function ϕ defined in region I and on its boundary S.

The wavefunction ϕ which minimizes (7) satisfies the following equation in region I, including S:

$$\begin{aligned} &\left(-\frac{1}{2}\nabla^2 + V(\mathbf{r})\right)\phi(\mathbf{r}) + \delta(\mathbf{r}-\mathbf{r}_S)\left[\frac{1}{2}\frac{\partial\phi}{\partial n_S}\right. \\ &+ \left.\int_S \mathrm{d}\mathbf{r}'_S\big(G_0^{-1}(\epsilon) + (E-\epsilon)\frac{\partial G_0^{-1}}{\partial\epsilon}\big)\phi(\mathbf{r}'_S)\right] = E\phi(\mathbf{r}). \end{aligned} \tag{8}$$

The embedding potential evaluated at trial energy ϵ plus the energy derivative term give G_0^{-1} at the required energy E, to first order in $(E-\epsilon)$. The surface terms in square brackets vanish when ϕ has the correct normal derivative to match on to the solution of the Schrödinger equation in region II, so this is the correctly embedded solution of the Schrödinger equation.

To find the solutions of (7) and (8), we expand ϕ in terms of basis functions χ_i (here we assume that they are real and orthonormal):

$$\phi(\mathbf{r}) = \sum_i a_i\chi_i(\mathbf{r}). \tag{9}$$

Substituting into (7) and finding the stationary values of E gives the following embedded Schrödinger equation in matrix form:

$$\sum_j (H_{ij} + \Sigma_{ij})a_j = Ea_i. \tag{10}$$

The first term comes from the Hamiltonian and the surface derivative term in the variational principle,

$$\begin{aligned} H_{ij} &= \int_I \mathrm{d}\mathbf{r}\,\chi_i(\mathbf{r})\left[-\frac{1}{2}\nabla^2 + V(\mathbf{r})\right]\chi_j(\mathbf{r}) \\ &\quad + \frac{1}{2}\int_S \mathrm{d}\mathbf{r}_S\,\chi_i(\mathbf{r}_S)\frac{\partial\chi_j(\mathbf{r}_S)}{\partial n_S} \\ &= \frac{1}{2}\int_I \mathrm{d}\mathbf{r}\,\nabla\chi_i(\mathbf{r})\cdot\nabla\chi_j(\mathbf{r}) + \int_I \mathrm{d}\mathbf{r}\,\chi_i(\mathbf{r})V(\mathbf{r})\chi_j(\mathbf{r}), \end{aligned} \tag{11}$$

while the second term comes from the embedding potential,

$$\begin{aligned} \Sigma_{ij} = &\int_S \mathrm{d}\mathbf{r}_S\int_S \mathrm{d}\mathbf{r}'_S\,\chi_i(\mathbf{r}_S)\left[G_0^{-1}(\mathbf{r}_S, \mathbf{r}'_S; \epsilon) + (E-\epsilon)\right. \\ &\times\left.\frac{\partial G_0^{-1}(\mathbf{r}_S, \mathbf{r}'_S; \epsilon)}{\partial\epsilon}\right]\chi_j(\mathbf{r}'_S). \end{aligned} \tag{12}$$

When ϵ lies in an energy continuum of region II, G_0^{-1} is complex, so we usually find the Green function of $(H+\Sigma)$ rather than the eigenvectors.

2.2. Time-dependent embedding

We shall now build the time-dependent formalism on the results of the last section. First we consider the relationships between normal derivative and amplitude as functions of time, corresponding to (3) and (4) in the energy-dependent case. Taking the Fourier transform of (3) gives us

$$\tilde{\psi}(\mathbf{r}_S, t) = -\frac{1}{2}\int_S \mathrm{d}\mathbf{r}'_S\int_{-\infty}^{t}\mathrm{d}t'\,\tilde{G}_0(\mathbf{r}_S, \mathbf{r}'_S; t-t')\frac{\partial\tilde{\psi}(\mathbf{r}'_S, t')}{\partial n_S} \tag{13}$$

where we use a tilde to indicate functions of time. $\tilde{G}_0$ satisfies the time-dependent Schrödinger equation in region II,

$$\left(-\frac{1}{2}\nabla^2 + V(\mathbf{r}) - \mathrm{i}\frac{\partial}{\partial t}\right)\tilde{G}_0(\mathbf{r}, \mathbf{r}'; t-t') = \delta(\mathbf{r}-\mathbf{r}')\delta(t-t'), \tag{14}$$

with the zero-derivative boundary condition on S, and, because we take the retarded Green function, we have,

$$\tilde{G}_0(\mathbf{r}, \mathbf{r}'; t-t') = 0, \qquad t < t', \tag{15}$$

hence the upper limit of t in the integral in (13). This can be derived directly by applying Green's theorem to the inhomogeneous equation (14), and the corresponding homogeneous equation for $\tilde{\psi}(\mathbf{r}, t)$ [8].

Turning to the inverse relation giving the derivative in terms of the amplitude, we have to proceed differently, because the Fourier transform of G_0^{-1} does not converge—it is an increasing function of ϵ. However, Ehrhardt [18] and Boucke *et al* [8] have shown that $\partial\tilde{\psi}(t)/\partial n_S$ can be expressed in terms of the time derivative of $\tilde{\psi}(t)$, and here we give a simple derivation. We re-write the integrand in (4) as

$$\int_S \mathrm{d}\mathbf{r}'_S \frac{G_0^{-1}(\mathbf{r}_S, \mathbf{r}'_S; \epsilon)}{-\mathrm{i}\epsilon}[-\mathrm{i}\epsilon\psi(\mathbf{r}'_S, \epsilon)]. \tag{16}$$

The Fourier transform of $G_0^{-1}(\epsilon)/-\mathrm{i}\epsilon$ converges, and the transform of $-\mathrm{i}\epsilon\psi(\epsilon)$ is $\partial\tilde{\psi}(t)/\partial t$. Defining $\bar{G}_0^{-1}(t)$ as the following Fourier transform,

$$\bar{G}_0^{-1}(\mathbf{r}_S, \mathbf{r}'_S; t) = \frac{1}{2\pi}\int_{-\infty}^{+\infty} \mathrm{d}\epsilon \exp(-\mathrm{i}\epsilon t)\frac{G_0^{-1}(\mathbf{r}_S, \mathbf{r}'_S; \epsilon)}{-\mathrm{i}\epsilon}, \tag{17}$$

the Dirichlet-to-Neumann equation in time becomes

$$\frac{\partial\tilde{\psi}(\mathbf{r}_S, t)}{\partial n_S} = -2\int_S \mathrm{d}\mathbf{r}'_S \int_{-\infty}^{t} \mathrm{d}t' \bar{G}_0^{-1}(\mathbf{r}_S, \mathbf{r}'_S; t-t')\frac{\partial\tilde{\psi}(\mathbf{r}'_S, t')}{\partial t'}. \tag{18}$$

We now turn to the embedding problem. The wavefunction satisfying the time-dependent equation, at this stage with a time-*independent* potential, can be written in region I in terms of solutions of the embedded Schrödinger equation (8),

$$\tilde{\phi}(\mathbf{r}, t) = \sum_i a_i\phi_i(\mathbf{r})\mathrm{e}^{-\mathrm{i}E_i t}. \tag{19}$$

Equation (8) simplifies if the embedding potential is evaluated at the eigen-energy,

$$\left(-\frac{1}{2}\nabla^2 + V(\mathbf{r})\right)\phi_i(\mathbf{r}) + \delta(\mathbf{r}-\mathbf{r}_S)\left[\frac{1}{2}\frac{\partial\phi_i}{\partial n_S} + \int_S \mathrm{d}\mathbf{r}'_S G_0^{-1}(E_i)\phi_i(\mathbf{r}'_S)\right] = E_i\phi_i(\mathbf{r}), \tag{20}$$

and multiplying this equation by the coefficients in (19) and summing over i gives

$$\left(-\frac{1}{2}\nabla^2 + V(\mathbf{r})\right)\tilde{\phi}(\mathbf{r}, t) + \delta(\mathbf{r}-\mathbf{r}_S)\left[\frac{1}{2}\frac{\partial\tilde{\phi}}{\partial n_S} + \int_S \mathrm{d}\mathbf{r}'_S \sum_i a_i G_0^{-1}(\mathbf{r}_S, \mathbf{r}'_S; E_i)\phi_i(\mathbf{r}'_S)\mathrm{e}^{-\mathrm{i}E_i t}\right] = \mathrm{i}\frac{\partial\tilde{\phi}}{\partial t}. \tag{21}$$

Using the same trick as in going from (16) to (17), this becomes

$$\left(-\frac{1}{2}\nabla^2 + V(\mathbf{r})\right)\tilde{\phi}(\mathbf{r}, t) + \delta(\mathbf{r}-\mathbf{r}_S)\left[\frac{1}{2}\frac{\partial\tilde{\phi}}{\partial n_S} + \int_S \mathrm{d}\mathbf{r}'_S \int_{-\infty}^{t} \mathrm{d}t' \bar{G}_0^{-1}(\mathbf{r}_S, \mathbf{r}'_S; t-t')\frac{\partial\tilde{\phi}(\mathbf{r}'_S, t')}{\partial t'}\right] = \mathrm{i}\frac{\partial\tilde{\phi}}{\partial t}, \tag{22}$$

an equation which holds for $\mathbf{r}$ inside region I and on the boundary S.

To show how the embedding terms in (22) work, we construct the solution of the time-dependent equation in region II, $\tilde{\psi}$, with the inhomogeneous boundary condition that it matches in amplitude on to $\tilde{\phi}$ over S, at all times up to t:

$$\tilde{\psi}(\mathbf{r}_S, t') = \tilde{\phi}(\mathbf{r}_S, t'), \qquad t' \leqslant t. \tag{23}$$

From (18), the normal derivative on S is given by

$$\frac{\partial\tilde{\psi}(\mathbf{r}_S, t)}{\partial n_S} = -2\int_S \mathrm{d}\mathbf{r}'_S \int_{-\infty}^{t} \mathrm{d}t' \bar{G}_0^{-1}(\mathbf{r}_S, \mathbf{r}'_S; t-t')\frac{\partial\tilde{\phi}(\mathbf{r}'_S, t')}{\partial t'}. \tag{24}$$

But the right-hand side is the second term in the square brackets in (22), with a factor of -2. For (22) to be satisfied on S as well as inside region I, the two terms in the square brackets must cancel, forcing $\tilde{\phi}(\mathbf{r}, t)$ to match in normal derivative on to the solution in II; as they already match in amplitude by construction, we have the correctly embedded solution of the time-dependent equation. Moreover, the normal derivative term combined with $-\frac{1}{2}\nabla^2$ gives a Hermitian operator when integrating over region I.

It is convenient to start off the time evolution at $t = 0$, assuming that

$$\tilde{\phi}(\mathbf{r}_S, t) = 0, \qquad t < 0, \tag{25}$$

so we change the lower limit in the embedding term in (22) from $-\infty$ to $t = 0$. We also allow the potential in region I to be a function of time—we can presumably do this, as it does not affect the surface integral, originating from region II. This gives us the final form of the embedded time-dependent Schrödinger equation:

$$\left(-\frac{1}{2}\nabla^2 + V(\mathbf{r}, t)\right)\tilde{\phi}(\mathbf{r}, t) + \delta(\mathbf{r}-\mathbf{r}_S)\left[\frac{1}{2}\frac{\partial\tilde{\phi}}{\partial n_S} + \int_S \mathrm{d}\mathbf{r}'_S \int_0^{t} \mathrm{d}t' \bar{G}_0^{-1}(\mathbf{r}_S, \mathbf{r}'_S; t-t')\frac{\partial\tilde{\phi}(\mathbf{r}'_S, t')}{\partial t'}\right] = \mathrm{i}\frac{\partial\tilde{\phi}}{\partial t}. \tag{26}$$

As in the time-independent case, this equation can be solved using a basis set expansion of $\tilde{\phi}(\mathbf{r}, t)$:

$$\tilde{\phi}(\mathbf{r}, t) = \sum_i a_i(t)\chi_i(\mathbf{r}). \tag{27}$$

Substituting into (26), we obtain the matrix form of the embedded Schrödinger equation,

$$\sum_j \left(H_{ij}(t)a_j(t) + \int_0^t \mathrm{d}t' \bar{\Sigma}_{ij}(t-t')\frac{\mathrm{d}a_j}{\mathrm{d}t'}\right) = \mathrm{i}\frac{\mathrm{d}a_i}{\mathrm{d}t}, \tag{28}$$

with the Hamiltonian matrix given by

$$H_{ij}(t) = \frac{1}{2}\int_I \mathrm{d}\mathbf{r}\, \nabla\chi_i(\mathbf{r})\cdot\nabla\chi_j(\mathbf{r}) + \int_I \mathrm{d}\mathbf{r}\, \chi_i(\mathbf{r})V(\mathbf{r}, t)\chi_j(\mathbf{r}), \tag{29}$$

and the embedding matrix by

$$\bar{\Sigma}_{ij}(t) = \int_S \mathrm{d}\mathbf{r}_S \int_S \mathrm{d}\mathbf{r}'_S\, \chi_i(\mathbf{r}_S)\bar{G}_0^{-1}(\mathbf{r}_S, \mathbf{r}'_S; t)\chi_j(\mathbf{r}'_S). \tag{30}$$

The structure of (26) and (28) is the same as in the spatially discretized approach to the problem [12, 20], with an embedding operator added on to the time-dependent Schrödinger equation.

3. The time-dependent embedding kernel

In this section we shall evaluate the embedding kernel $\bar{G}_0^{-1}(t)$ for constant and linear potentials in region II. We work in one dimension, but we shall see in section 3.3 how the results can be applied to three-dimensional problems.

3.1. Embedding on to zero potential

In the one-dimensional case we use (4) to determine $G_0^{-1}(\epsilon)$, and then substitute into the Fourier transform (17) to find $\bar{G}_0^{-1}(t)$. With zero potential the wavefunctions in region II satisfying outgoing boundary conditions for $z \geqslant 0$ are

$$\psi(z,\epsilon) = \begin{cases} \exp(-\gamma z), & \gamma = \sqrt{-2\epsilon}, \quad \epsilon < 0 \\ \exp(\mathrm{i}\kappa z), & \kappa = \sqrt{2\epsilon}, \quad \epsilon > 0. \end{cases} \tag{31}$$

Hence the embedding potential is

$$G_0^{-1}(\epsilon) = \sqrt{-\epsilon/2} \quad \text{or} \quad -\mathrm{i}\sqrt{\epsilon/2}, \tag{32}$$

and substituting into (17) the time-dependent embedding kernel is given by

$$\bar{G}_0^{-1}(t) = \frac{1}{2\pi}\int_{-\infty}^{+\infty} \mathrm{d}\epsilon \exp(-\mathrm{i}\epsilon t) \begin{cases} \dfrac{-\mathrm{i}}{\sqrt{-2\epsilon}}, & \epsilon < 0 \\ \dfrac{1}{\sqrt{2\epsilon}}, & \epsilon > 0. \end{cases} \tag{33}$$

This integral can be performed analytically [8], and the result is

$$\bar{G}_0^{-1}(t) = \begin{cases} 0, & t < 0 \\ \dfrac{1-i}{2\sqrt{\pi}} \cdot \dfrac{1}{\sqrt{t}}, & t > 0. \end{cases} \tag{34}$$

We shall apply this embedding kernel in applications in sections 4 and 5.

3.2. Embedding on to an electric field

With other one-dimensional potentials it is necessary to carry out the Fourier transform in (17) numerically, and we consider the linear potential corresponding to a constant electric field $\mathcal{E}$. The wavefunctions in region II satisfy the Schrödinger equation,

$$-\frac{1}{2}\frac{\mathrm{d}^2\psi}{\mathrm{d}z^2} - \mathcal{E}z\psi = \epsilon\psi, \tag{35}$$

which has Airy function solutions [25],

$$\begin{aligned} \psi_1(z) &= \mathrm{Ai}\left(-(2\mathcal{E})^{\frac{1}{3}}(z+\epsilon/\mathcal{E})\right), \\ \text{and} \quad \psi_2(z) &= \mathrm{Bi}\left(-(2\mathcal{E})^{\frac{1}{3}}(z+\epsilon/\mathcal{E})\right). \end{aligned} \tag{36}$$

Now we need the combination of ψ_1 and ψ_2 corresponding to outgoing waves, and from the asymptotic behaviour of the Airy functions [25], this is given by

$$\psi_+(z) = \mathrm{Bi}\left(-(2\mathcal{E})^{\frac{1}{3}}(z+\epsilon/\mathcal{E})\right) + \mathrm{iAi}\left(-(2\mathcal{E})^{\frac{1}{3}}(z+\epsilon/\mathcal{E})\right). \tag{37}$$

So in this case the energy-dependent embedding potential at $z = 0$ is

$$G_0^{-1}(\epsilon) = \frac{(2\mathcal{E})^{\frac{1}{3}}\left[\mathrm{Bi}'\left(-(2\mathcal{E})^{\frac{1}{3}}\epsilon/\mathcal{E}\right) + \mathrm{iAi}'\left(-(2\mathcal{E})^{\frac{1}{3}}\epsilon/\mathcal{E}\right)\right]}{2\left[\mathrm{Bi}\left(-(2\mathcal{E})^{\frac{1}{3}}\epsilon/\mathcal{E}\right) + \mathrm{iAi}\left(-(2\mathcal{E})^{\frac{1}{3}}\epsilon/\mathcal{E}\right)\right]}, \tag{38}$$

which we evaluate using the Airy function programs due to Gil *et al* [26]. For large positive or negative ϵ, $G_0^{-1}(\epsilon)$ has the $\sqrt{\epsilon}$ free-electron behaviour given by equation (32), so once again we divide by ϵ when finding the Fourier transform to obtain the time-dependent kernel. The free-electron behaviour at large ϵ is what we would expect—the potential becomes irrelevant in this limit.

In the numerical Fourier transform of $G_0^{-1}(\epsilon)/\epsilon$ we must be careful about the singularity at $\epsilon = 0$, and we re-write the integral as

$$\begin{aligned} \bar{G}_0^{-1}(t) &= \frac{\mathrm{i}}{2\pi}\int_{-\infty}^{+\infty} \mathrm{d}\epsilon \exp(-\mathrm{i}\epsilon t)\frac{G_0^{-1}(\epsilon)}{\epsilon} \\ &= \frac{\mathrm{i}}{2\pi}\int_{-\infty}^{+\infty} \mathrm{d}\epsilon \exp(-\mathrm{i}\epsilon t)\frac{G_0^{-1}(\epsilon) - G_0^{-1}(0)}{\epsilon} \\ &\quad + \frac{\mathrm{i}G_0^{-1}(0)}{2\pi}\int_{-\infty}^{+\infty} \mathrm{d}\epsilon \frac{\exp(-\mathrm{i}\epsilon t)}{\epsilon}. \end{aligned} \tag{39}$$

The first integral is well behaved at $\epsilon = 0$, but in evaluating the second integral we have to be careful about the contour of integration around this point. As $\bar{G}_0^{-1}(t)$ is zero for $t < 0$, the singularities of the integrand must lie in the lower half-plane, so we replace $\frac{1}{\epsilon}$ by $\frac{1}{\epsilon+\mathrm{i}\eta}$, where η is infinitesimal. Our Fourier transform then becomes

$$\begin{aligned} \bar{G}_0^{-1}(t) &= \frac{\mathrm{i}}{2\pi}\int_{-\infty}^{+\infty} \mathrm{d}\epsilon \exp(-\mathrm{i}\epsilon t)\frac{G_0^{-1}(\epsilon) - G_0^{-1}(0)}{\epsilon} \\ &\quad + \begin{cases} 0, & t < 0 \\ G_0^{-1}(0), & t > 0. \end{cases} \end{aligned} \tag{40}$$

To evaluate the integral in (40), our procedure is to include an exponential damping term $\exp(-|\epsilon|/\Gamma)$, and discretize the integral with finite limits. This simple method of evaluating the Fourier transform works well.

Results for the time-dependent embedding kernel with an electric field $\mathcal{E} = 2$ au are shown in figure 2, using a coefficient $\Gamma = 500$ au in the damping term. We see that $\bar{G}_0^{-1}(t)$ is accurately zero for negative t. For $t \to 0$ from above, the kernel tends to the free-electron value (34), in accordance with our intuition: at short times (or high energies) an electron cannot tell whether it is in an electric field or not. For larger t, $\bar{G}_0^{-1}(t)$ rapidly approaches the zero-frequency embedding potential, $G_0^{-1}(0)$, which is the contribution from the pole in the frequency integral (39); the larger the field, the more rapidly it approaches a constant value. This form of $\bar{G}_0^{-1}(t)$ makes it very easy to evaluate the long-time contribution to the embedded Schrödinger equation.

We test the accuracy of the embedding kernel by calculating the time evolution of a wavefunction $\tilde{\psi}(z,t)$ over the extended system of regions I and II, and then use (18) to compare the Dirichlet-to-Neumann result with the directly calculated derivative at the boundary of region II. In this

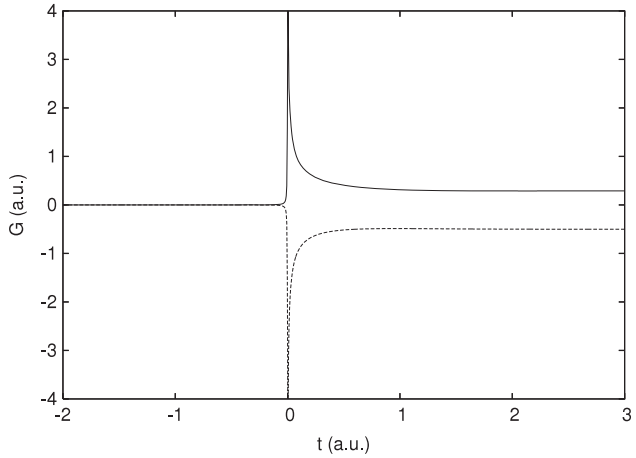

Figure 2. $\bar{G}_0^{-1}(t)$ for the Schrödinger equation with electric field $\mathcal{E} = 2$ au: solid line, Re $\bar{G}_0^{-1}$; dashed line, Im $\bar{G}_0^{-1}$.

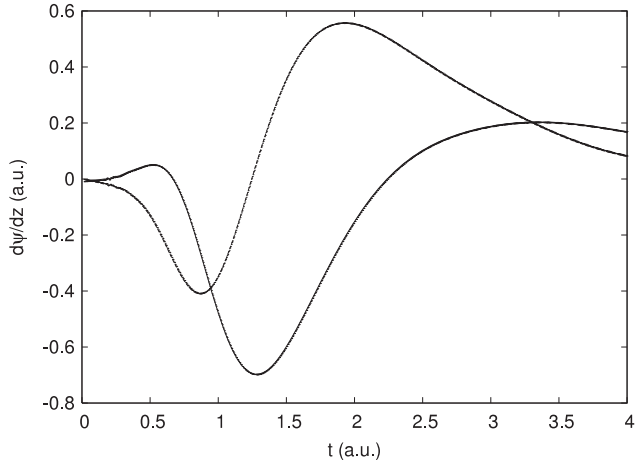

Figure 3. Electric field test: $\partial\tilde{\psi}/\partial z$ at z' evaluated from the Dirichlet-to-Neumann relation compared with direct calculation from the numerical wavefunction. D-to-N results are the solid line (real part) and the dashed line (imaginary part); direct results are the dots, which are hardly distinguishable except close to $t = 0$.

test the potential itself is time-independent, with an infinite barrier at $z = 0$, zero potential between $z = 0$ and z', and in region II beyond z' an electric field corresponding to the potential $-\mathcal{E}(z - z')$. The wavefunction at $t = 0$ is taken to be a sum of Gaussians vanishing at $z = 0$,

$$\tilde{\psi}(z, 0) = \exp\left[-\left(\frac{z - z_0}{w}\right)^2\right] - \exp\left[-\left(\frac{z + z_0}{w}\right)^2\right], \quad z > 0, \tag{41}$$

and the value of z_0 and the width w are chosen so that the initial value of the wavefunction at z', where the electric field starts, is negligible. To solve the time-dependent Schrödinger equation for $\tilde{\psi}(z, t)$ we discretize in both space and time, evolving forward in time steps δt using the norm-conserving Crank–Nicolson method [29],

$$\tilde{\psi}(z, t + \delta t) = \left(1 + \frac{\mathrm{i}\delta t H}{2}\right)^{-1}\left(1 - \frac{\mathrm{i}\delta t H}{2}\right)\tilde{\psi}(z, t), \tag{42}$$

where H is the finite-difference Hamiltonian matrix [30].

For this test we take an electric field $\mathcal{E} = 2$ au beyond $z' = 3$ au, with the constants in the Gaussian wavefunction $z_0 = 0.5$ au, $w = 1$ au. The intervals in the spatial and time discretization are $\delta z = 0.0005$ au and $\delta t = 0.005$ au, and the spatial range extends to $z = 40$ au—enough to eliminate edge effects over the time range that we consider. We then evaluate $\partial\tilde{\psi}/\partial z$ at z' directly from the finite-difference results, using first-order differences, and compare this with the derivative evaluated using (18) with the embedding kernel shown in figure 2, and first-order differences for $\partial\tilde{\psi}/\partial t$. The comparison is shown in figure 3: the values of $\partial\tilde{\psi}/\partial z$ from the Dirichlet-to-Neumann (D-to-N) relationship (solid and dashed lines) can hardly be distinguished from the results for the derivative calculated directly (dots). Only at very short times, and because of some noise in the direct results, can they be distinguished. This shows that our numerical evaluation of the embedding kernel for the electric field is accurate—the method can presumably be extended to other potentials.

3.3. Shifting the potential

If we know the embedding kernel for a potential $V(\mathbf{r})$ in region II, we can immediately find an expression analogous to the Dirichlet-to-Neumann relationship (18) for the potential shifted by a constant V_0. The time-dependent Schrödinger equation satisfied by $\tilde{\psi}(\mathbf{r}, t)$ in region II is given by

$$\left(-\frac{1}{2}\nabla^2 + V(\mathbf{r}) + V_0\right)\tilde{\psi}(\mathbf{r}, t) = \mathrm{i}\frac{\partial\tilde{\psi}}{\partial t}, \tag{43}$$

and making the substitution

$$\tilde{\psi}(\mathbf{r}, t) = \exp(-\mathrm{i}V_0 t)\tilde{\Psi}(\mathbf{r}, t), \tag{44}$$

$\tilde{\Psi}$ satisfies the unshifted Schrödinger equation

$$\left(-\frac{1}{2}\nabla^2 + V(\mathbf{r})\right)\tilde{\Psi}(\mathbf{r}, t) = \mathrm{i}\frac{\partial\tilde{\Psi}}{\partial t}. \tag{45}$$

As $\partial\tilde{\Psi}/\partial n_S$ is related to $\partial\tilde{\Psi}/\partial t$ by the original embedding kernel for $V(\mathbf{r})$, the corresponding relationship for $\tilde{\psi}$ with the shifted potential is given by

$$\frac{\partial\tilde{\psi}(\mathbf{r}_S, t)}{\partial n_S} = -2\exp(-\mathrm{i}V_0 t)\int_S \mathrm{d}\mathbf{r}'_S \int_0^t \mathrm{d}t' \bar{G}_0^{-1}(\mathbf{r}_S, \mathbf{r}'_S; t - t') \times \frac{\partial}{\partial t'}[\exp(\mathrm{i}V_0 t')\tilde{\psi}(\mathbf{r}'_S, t')]. \tag{46}$$

This result will be particularly useful when we come to deal with the potential step at a surface. Moreover, a one-dimensional potential has often been used in surface calculations [27], and then the solutions of the Schrödinger equation have the form

$$\tilde{\psi}(\mathbf{r}, t) = \exp(\mathrm{i}\mathbf{K}\cdot\mathbf{R})\hat{\psi}_K(z, t), \tag{47}$$

where $\mathbf{K}$ is the Bloch wavevector parallel to the surface, and $\mathbf{R}$ is the surface-parallel component of $\mathbf{r}$. Then $\hat{\psi}_K$ satisfies the

one-dimensional Schrödinger equation shifted by $K^2/2$, and the Dirichlet-to-Neumann relationship becomes

$$\frac{\partial \hat{\psi}_K(z,t)}{\partial z} = -2\exp\left(-\frac{\mathrm{i}K^2 t}{2}\right)\int_0^t \mathrm{d}t' \bar{G}_0^{-1}(t-t') \times \frac{\partial}{\partial t'}\left[\exp\left(\frac{\mathrm{i}K^2 t'}{2}\right)\hat{\psi}_K(z,t')\right], \tag{48}$$

where $\bar{G}_0^{-1}$ is the embedding kernel for the one-dimensional potential. The right-hand side of (48) provides the embedding potential for states with Bloch wavevector **K** in this form of potential.

Another approximation for surfaces is to assume the full three-dimensional potential for the surface region itself (region I) and a one-dimensional potential for the bulk substrate and the vacuum (which together constitute region II) [28]. Again, (48) can be used to construct the embedding potential for each Fourier component of the wavefunction in region I. We shall explore this in a later paper.

4. Embedding

4.1. Model atomic problem

To test our time-dependent embedding method with the kernels derived in section 3, in this section we calculate the time-evolution of states which are initially localized in region I. We start off with the time evolution of the normalized bound-state wavefunction $\psi(z) = 1/\sqrt{2}\cosh(z)$ of the one-dimensional potential $V(z) = -1/\cosh^2(z)$ in a time-varying electric field $\mathcal{E} = \mathcal{E}_0 \sin\omega t$. Ermolaev *et al* [22] solve this problem directly, but we follow Boucke *et al* [8], who use the Kramers–Henneberger transformation [21] to convert this into the problem of the wavefunction evolving in the oscillating potential,

$$V(z,t) = -1/\cosh^2[z + \xi_0 \sin(\omega t)] \tag{49}$$

with zero potential beyond (figure 4). Here ξ_0 is the classical amplitude of oscillation in the electric field, $\xi_0 = \mathcal{E}_0/\omega^2$. We solve the embedded Schrödinger equations (26), (28) in region I, defined as $|z| < d$, replacing the regions with $|z| > d$ by the zero-potential embedding kernel. The time-dependent wavefunction in region I, $\tilde{\phi}(z,t)$, is expanded in a basis set given by

$$\Xi_m = \begin{cases} \cos\dfrac{m\pi z}{2D}, & m \text{ even} \\ \sin\dfrac{m\pi z}{2D}, & m \text{ odd}, \end{cases} \tag{50}$$

where D lies beyond d (figure 4) to give flexibility in amplitude and derivative at the boundary of region I. We orthogonalize and normalize the basis functions within region I by diagonalizing the overlap matrix S_{mn},

$$S_{mn} = \int_{-d}^{+d} \mathrm{d}z\, \Xi_m(z)\Xi_n(z). \tag{51}$$

Defining α^j as the jth eigenvector of S, with eigenvalue s_j, the jth orthonormalized basis function is given by

$$\chi_j(z) = \frac{1}{\sqrt{s_j}}\sum_m \alpha_m^j\, \Xi_m(z). \tag{52}$$

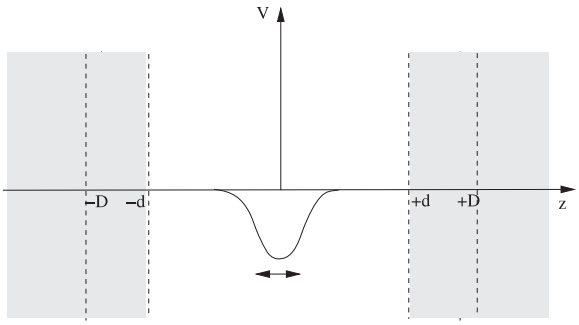

Figure 4. Oscillating model atomic potential. Region I, treated explicitly, lies within $z = \pm d$. The basis functions for expanding the wavefunction in region I are defined in terms of $z = \pm D$.

If overcompleteness is a problem, this will show itself as a very small value of s_j, and the corresponding basis function can be dropped.

The time-dependent matrix equation (28) becomes, in this one-dimensional case with embedding at both ends of the range,

$$\sum_j H_{ij}(t)a_j(t) + \chi_i(-d)\int_0^t \mathrm{d}t' \bar{G}_0^{-1}(t-t')\frac{\partial\tilde{\phi}(-d,t')}{\partial t'} + \chi_i(d)\int_0^t \mathrm{d}t' \bar{G}_0^{-1}(t-t')\frac{\partial\tilde{\phi}(d,t')}{\partial t'} = \mathrm{i}\frac{\mathrm{d}a_i}{\mathrm{d}t}, \tag{53}$$

where the Hamiltonian matrix element is given by

$$H_{ij}(t) = \int_{-d}^{+d}\mathrm{d}z\left(\frac{1}{2}\frac{\mathrm{d}\chi_i}{\mathrm{d}z}\frac{\mathrm{d}\chi_j}{\mathrm{d}z} + \chi_i(z)V(z,t)\chi_j(z)\right), \tag{54}$$

and the embedding kernel $\bar{G}_0^{-1}$ is given by (34).

We turn to the numerical time integration of (53), which we write as

$$\frac{\mathrm{d}a}{\mathrm{d}t} + \mathrm{i}Ha = -\mathrm{i}\Gamma, \tag{55}$$

where Γ is the vector representing the embedding terms in (53):

$$\Gamma_i = \chi_i(-d)\int_0^t \mathrm{d}t' \bar{G}_0^{-1}(t-t')\frac{\partial\tilde{\phi}(-d,t')}{\partial t'} + \chi_i(d)\int_0^t \mathrm{d}t' \bar{G}_0^{-1}(t-t')\frac{\partial\tilde{\phi}(d,t')}{\partial t'}. \tag{56}$$

We can improve on the first-order integration scheme,

$$a(t+\delta t) = [1 + \mathrm{i}\delta t H(t)]^{-1}[a(t) - \mathrm{i}\delta t\Gamma(t)], \tag{57}$$

by expanding the time-evolution operator to second order in δt, giving

$$a(t+\delta t) = \left(1 + \mathrm{i}\delta t H(t) - \frac{\delta t^2 H(t)^2}{2}\right)^{-1}[a(t) - \mathrm{i}\delta t\Gamma(t)]. \tag{58}$$

Although it is not consistently second order in δt, this stable scheme proves more accurate than (57) in our tests. In evaluating the integrals in (56) we use

$$\frac{\partial\tilde{\phi}(t)}{\partial t} \approx \frac{\tilde{\phi}(t) - \tilde{\phi}(t-\delta t)}{\delta t}, \tag{59}$$

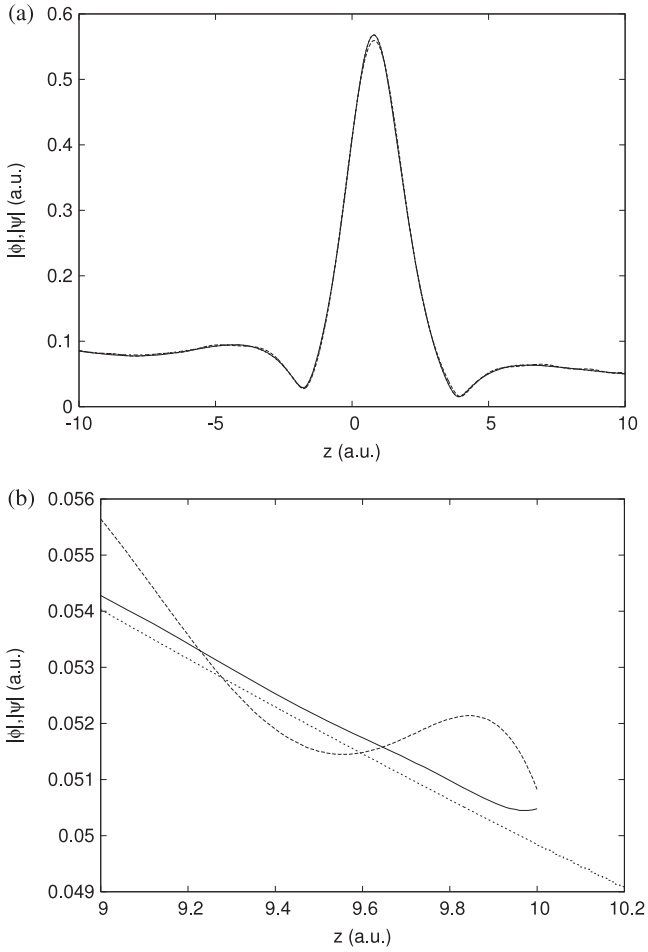

Figure 5. Oscillating potential: magnitude of wavefunction at $t = 80$ au, 2.55 periods. $|\tilde{\phi}|$ calculated using embedding: solid line, 40 basis functions; dashed line, 25 basis functions. $|\tilde{\psi}|$ calculated over extended space using finite differences: short-dashed line. (a) Plotted over embedding region between $z = \pm 10$ au. $|\tilde{\phi}|$ with 40 basis functions and $|\tilde{\psi}|$ are indistinguishable on this scale. (b) Plotted around the embedding point at $z = 10$ au.

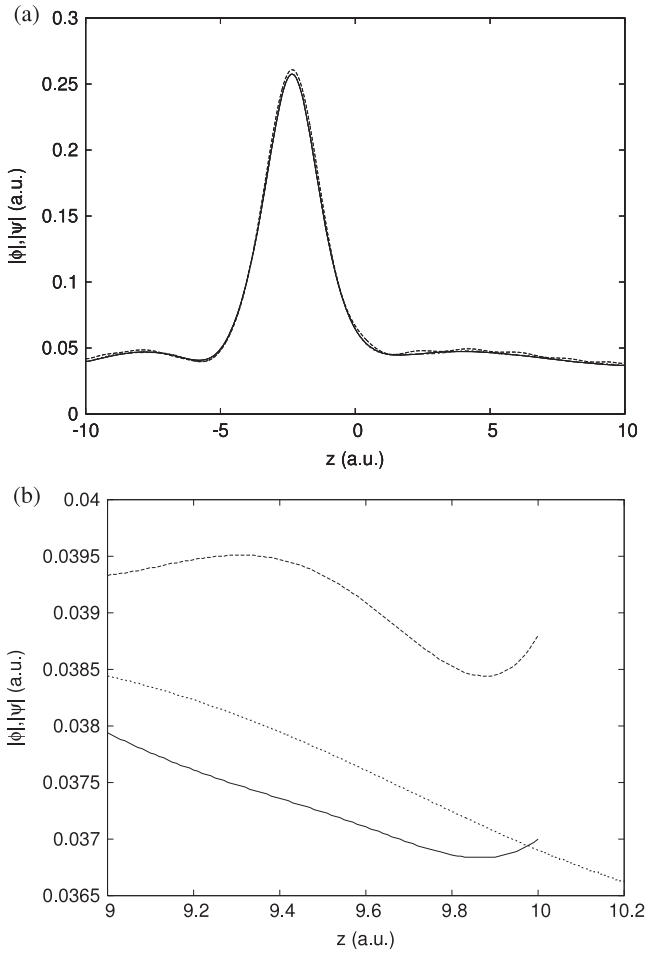

Figure 6. Oscillating potential: magnitude of wavefunction at $t = 320$ au, 10.19 periods. $|\tilde{\phi}|$ calculated using embedding: solid line, 40 basis functions; dashed line, 25 basis functions. $|\tilde{\psi}|$ calculated over extended space using finite differences: short-dashed line. (a) Plotted over embedding region between $z = \pm 10$ au. $|\tilde{\phi}|$ with 40 basis functions and $|\tilde{\psi}|$ are indistinguishable on this scale. (b) Plotted around the embedding point at $z = 10$ au.

rather than the more accurate formula

$$\frac{\partial \tilde{\phi}(t)}{\partial t} \approx \frac{\tilde{\phi}(t+\delta t) - \tilde{\phi}(t-\delta t)}{2\delta t}, \tag{60}$$

because (60) cannot be applied at the upper limit of the integral—we do not yet know $\tilde{\phi}(t + \delta t)$. To perform the integration itself, we subtract off the $(t - t')^{-1/2}$ singularity at $t' = t$, and then use the trapezium rule for the remaining well-behaved integral.

We calculate $\tilde{\phi}(z, t)$ in the oscillating potential (49), with an amplitude of oscillation $\xi_0 = 2.5$ au and frequency $\omega = 0.2$ au, corresponding to an electric field $\mathcal{E}_0 = 0.1$ au. (These are the values used by Boucke *et al* [8]—as the bound-state energy of the starting wavefunction is -0.5 au, ionization is due to multiphoton processes.) Region I is taken with $d = 10$ au, and the basis functions are defined with $D = 13$ au; the results presented below are for 25 and 40 basis functions. An interval $\delta t = 0.01$ au is used in the time integration (58). As a benchmark we compare the embedding results with the wavefunction $\tilde{\psi}(z, t)$ calculated over an extended range, using finite differences and Crank–Nicolson time integration (42) (throughout this section we use $\tilde{\psi}(z, t)$ to indicate the wavefunction through space extended beyond region I). The extended wavefunction is calculated over the range $-400 < z < 400$ au, with a spatial interval $\delta z = 0.004$ au, and a time interval $\delta t = 0.02$ au.

Figures 5, 6 and 7 show the comparison between the embedded and finite-difference wavefunctions in region I, for times $t = 80$, 320, and 400 au (the period of the oscillating potential is 31.42 au) and we see that the agreement is very good. At the scale of figures 5(a)–6(a), the magnitude of the embedded wavefunction $|\tilde{\phi}|$, calculated with 40 basis functions, is indistinguishable from the magnitude of the extended wavefunction $|\tilde{\psi}|$. From figures 5(b)–6(b), we see that the error in $|\tilde{\phi}|$ is about 5×10^{-4} au, with a slight decrease in accuracy with increasing time. The results with 25 basis functions are less accurate—they are just distinguishable from the extended results on the scale of figures 5(a) and 6(a). At

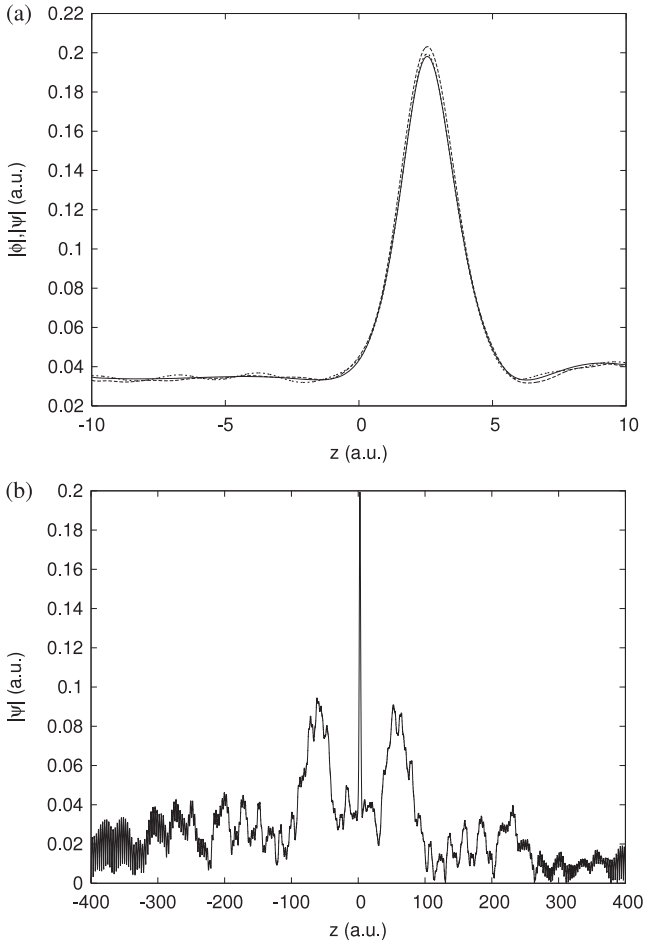

Figure 7. Oscillating potential: magnitude of wavefunction at $t = 400$ au., 12.73 periods. (a) $|\tilde{\phi}|$ calculated using embedding: solid line, 40 basis functions; dashed line, 25 basis functions. $|\tilde{\psi}|$ calculated over extended space using finite differences: short-dashed line. Plotted over embedding region between $z = \pm 10$ au. (b) $|\tilde{\psi}|$ plotted over extended region between $z = \pm 400$ au, showing reflection of the wavefunction at the boundaries of the finite-difference calculation, and subsequent interference.

$t = 400$ au, $|\tilde{\psi}|$ shows slight oscillations about the embedded $|\tilde{\phi}|$ with 40 basis functions (figure 7(a)). The reason for this is that the extended wavefunction has been reflected from the limits of its range at $z = \pm 400$ au, with resulting interference, as we can see from figure 7(b). Our embedding results are less accurate than those of Boucke *et al* [8], who achieve a relative accuracy in their embedded wavefunction of about 5×10^{-5}; however, they apply their embedding as a boundary condition on a much larger finite-difference calculation.

4.2. Surface excitation in a field

In this section we shall follow the time evolution of an electron wavefunction, initially in the $1/\sqrt{2}\cosh(z - z')$ bound state of a $-1/\cosh^2(z - z')$ potential near a surface, at which there is a constant applied electric field $\mathcal{E}$ (figure 8). The surface potential step $V_{\rm st}$ is broadened, so the static potential felt by

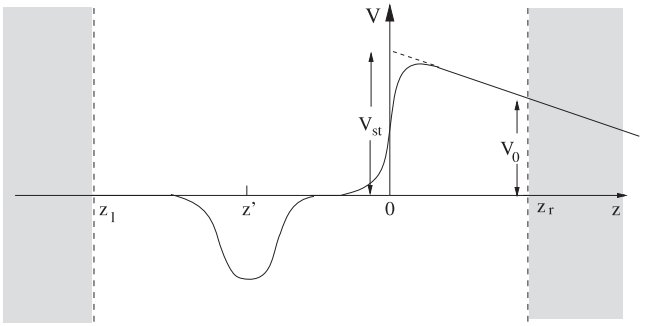

Figure 8. Model atomic potential near a jellium surface, with applied electric field in the vacuum. Region I, treated explicitly, lies within embedding boundaries at z_l and z_r.

the electron is given by

$$V(z) = -\frac{1}{\cosh^2(z - z')} + V_{\rm st}\left(\frac{1 + \tanh z/\xi}{2}\right) - \mathcal{E}z\theta(z), \tag{61}$$

where $\theta(z)$ is the step function. The surface parameters that we use are $V_{\rm st} = 0.5$ au and $\xi = 0.5$ au, and we position the 'atomic' potential at $z' = -4$ au. The electric field is $\mathcal{E} = 0.2$ au, approximately 10^{11} V m^{-1}—this is much larger than the fields used in field emission, but it could represent the field of an infrared laser in a quasi-static approximation. To excite the bound-state electron, an additional time-dependent potential is applied, of the form

$$\delta V(z, t) = a \exp -\left(\frac{z - z'}{\zeta}\right)^2 \sin(\omega t), \tag{62}$$

with $a = 1$ au, $\zeta = 2$ au, and frequency $\omega = 1$ au. This is turned on at $t = 0$, and we follow the subsequent time evolution of the bound-state electron wavefunction.

Region I lies in the surface region between the embedding boundaries at z_l and z_r (figure 8). We take $z_l = -14$ au and $z_r = 6$ au, so the embedding region extends ± 10 au on either side of the atomic potential. The Hamiltonian for region I is embedded on to the zero-potential embedding kernel (34) at z_l; at z_r it is embedded on to the Airy function kernel evaluated numerically (section 3.2), shifted by the constant potential V_0 (figure 8), using the shift formula (46). We use the basis functions given by (50) to expand the time-dependent wavefunction in region I — these are centred on the atomic potential with $D = 13$ au.

Results for $\tilde{\phi}(z, t)$ at $t = 50$ au are shown in figure 9(a), calculated with 25 basis functions, compared with a finite-difference calculation for $\tilde{\psi}(z, t)$ calculated over an extended range, $-400 < z < 400$ au (figure 9(b)). We see that agreement is very satisfactory, though not quite as good as in section 4.1 where we used an analytic embedding kernel. In this calculation we need to take $\delta t = 0.0025$ au in the time integration, compared with 0.01 au in section 4.1. This is probably because of the difference in the time-dependent perturbation.

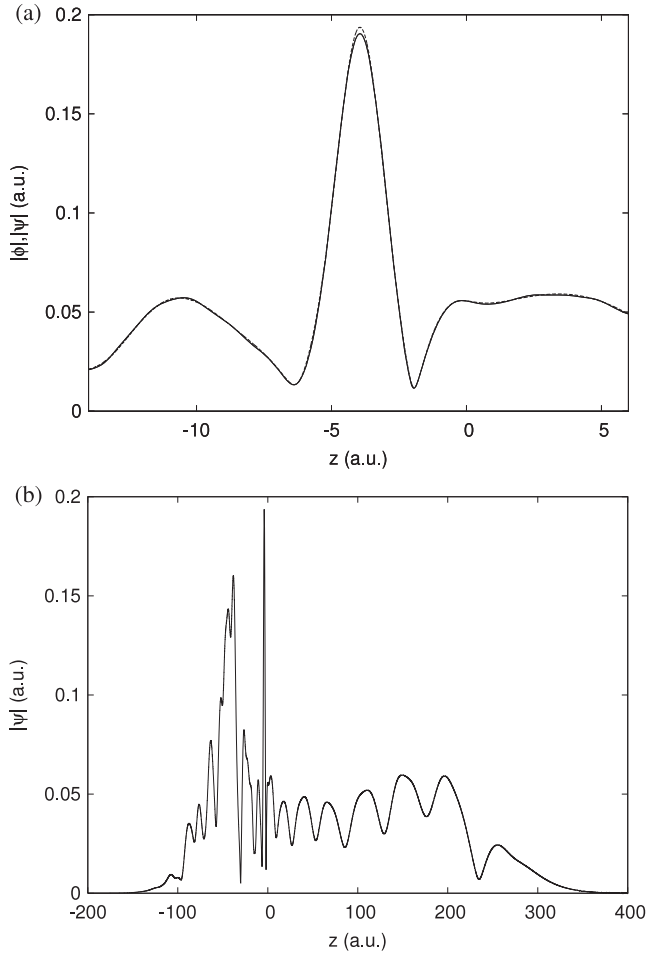

Figure 9. Excitation in a field, $\mathcal{E} = 0.2$ au: magnitude of wavefunction at $t = 50$ au. (a) $|\tilde{\phi}|$ calculated using embedding with 25 basis functions, solid line; $|\tilde{\psi}|$ calculated over extended space using finite differences, dashed line. Plotted over embedding region between $z = -14$ and 6 au. (b) $|\tilde{\psi}|$ plotted over extended region.

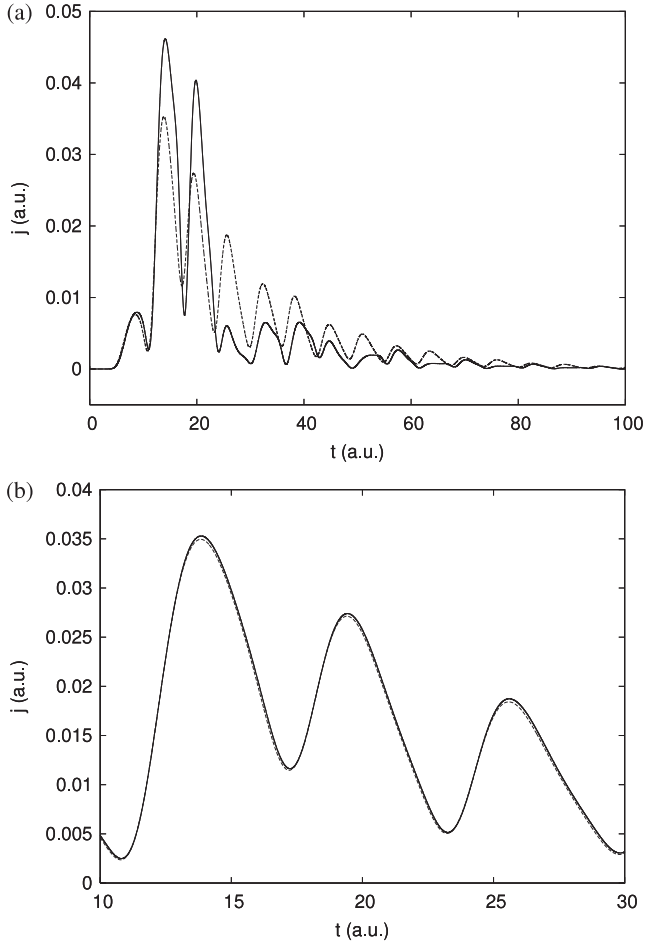

Figure 10. Excitation in a field, $\mathcal{E} = 0.2$ au: current across boundaries of region I as a function of time. (a) j calculated with embedding: solid line, across left-hand boundary at z_l; dashed line, across right-hand boundary at z_r. (b) Comparison of j at z_r using embedding (solid line), with finite differences (dashed line).

We also calculate the current crossing the embedding boundaries at z_l and z_r, using the expression

$$j(z,t) = \mathrm{Im}\left(\tilde{\phi}^* \frac{\partial \tilde{\phi}}{\partial z}\right), \tag{63}$$

with the normal derivative determined from the embedding formula (18). Taking the derivative outward from region I, a positive current indicates charge leaving the region. Our results are shown in figure 10(a) for the current crossing each boundary as a function of time—here we have something physical, which could in principle be compared with experiment. There is excellent agreement with the current calculated from the finite-difference results, as we see from figure 10(b), giving the current in the time range where there is the biggest difference between the two methods.

5. Time evolution of extended states

The formalism developed up to now assumes that the wavefunction $\tilde{\phi}(\mathbf{r}, t)$, whose time evolution we study in region I, has zero amplitude for $t < 0$ at the embedding surface and in region II. But in condensed matter applications we are usually interested in exciting bulk states to which this condition does not apply, and to study their time evolution we have to extend the formalism.

We start with a wavefunction $\Psi(\mathbf{r})$ which is an eigenstate with energy E of the time-independent Hamiltonian H_0, extending through regions I and II. For times $t > 0$ a time-dependent perturbing potential $\delta V(\mathbf{r}, t)$ is applied—confined to region I—and the wavefunction is subsequently given throughout space by

$$\tilde{\psi}(\mathbf{r}, t) = \Psi(\mathbf{r}) \exp(-\mathrm{i}Et) + \tilde{\eta}(\mathbf{r}, t). \tag{64}$$

Substituting into the time-dependent Schrödinger equation gives

$$[H_0 + \delta V(t)]\tilde{\eta}(t) + \delta V(t)\Psi \exp(-\mathrm{i}Et) = \mathrm{i}\frac{\partial \tilde{\eta}}{\partial t}, \tag{65}$$

so $\tilde{\eta}(\mathbf{r}, t)$ satisfies the time-dependent Schrödinger equation with an additional inhomogeneous term. In region II, where

$\delta V = 0$, this term vanishes and $\tilde{\eta}$ satisfies the original Schrödinger equation,

$$H_0\tilde{\eta}(t) = \mathrm{i}\frac{\partial\tilde{\eta}}{\partial t}, \tag{66}$$

so $\tilde{\eta}$ and its normal derivative across S are related by the Dirichlet-to-Neumann result (18),

$$\frac{\partial\tilde{\eta}(\mathbf{r}_\mathrm{S},t)}{\partial n_\mathrm{S}} = -2\int_\mathrm{S}\mathrm{d}\mathbf{r}'_\mathrm{S}\int_0^t \mathrm{d}t'\bar{G}_0^{-1}(\mathbf{r}_\mathrm{S},\mathbf{r}'_\mathrm{S};t-t')\frac{\partial\tilde{\eta}(\mathbf{r}'_\mathrm{S},t')}{\partial t'}. \tag{67}$$

This means that we can write a time-dependent Schrödinger equation for $\tilde{\eta}(\mathbf{r},t)$ analogous to (26), with the extra inhomogeneous term,

$$\begin{aligned}&\left(-\tfrac{1}{2}\nabla^2 + V_0(\mathbf{r}) + \delta V(\mathbf{r},t)\right)\tilde{\eta}(\mathbf{r},t) + \delta V(\mathbf{r},t)\Psi(\mathbf{r})\\ &\quad\times\exp(-\mathrm{i}Et) + \delta(\mathbf{r}-\mathbf{r}_\mathrm{S})\left[\frac{1}{2}\frac{\partial\tilde{\eta}}{\partial n_\mathrm{S}} + \int_\mathrm{S}\mathrm{d}\mathbf{r}'_\mathrm{S}\int_0^t\mathrm{d}t'\right.\\ &\quad\left.\times\bar{G}_0^{-1}(\mathbf{r}_\mathrm{S},\mathbf{r}'_\mathrm{S};t-t')\frac{\partial\tilde{\eta}(\mathbf{r}'_\mathrm{S},t')}{\partial t'}\right] = \mathrm{i}\frac{\partial\tilde{\eta}}{\partial t}.\end{aligned} \tag{68}$$

Solving this equation within region I gives us the change in bulk wavefunction. Note that in this section we use $\tilde{\eta}(\mathbf{r},t)$ for the change in wavefunction with $\mathbf{r}$ in region I, evaluated by embedding (analogous to $\tilde{\phi}$ in previous sections), as well as the change in wavefunction extended through all space (analogous to $\tilde{\psi}$).

As a model problem we consider the jellium surface with a smeared-out potential step,

$$V_0(z) = V_\mathrm{st}\left(\frac{1+\tanh z/\xi}{2}\right), \tag{69}$$

using the same parameters as in section 4.2: $V_\mathrm{st} = 0.5$ au, $\xi = 0.5$ au. Region I lies within embedding boundaries at $z_l = -10$ au and $z_r = 10$ au, beyond which the potential is taken as constant. The bulk continuum wavefunction is found numerically using Numerov's method [30], matching $\Psi(z)$ on to the asymptotic solutions of the time-independent Schrödinger equation

$$\Psi(z) = \begin{cases}\sin(kz+\phi), & z < z_l\\ \alpha\exp(-\gamma z), & z > z_r,\end{cases} \tag{70}$$

with

$$k = \sqrt{2E}, \qquad \gamma = \sqrt{2(V_\mathrm{st}-E)}. \tag{71}$$

We use the same time-dependent perturbing potential as in section 4.2 (62), but in this case centred at the surface step. Region I is embedded at z_l on to the free-electron embedding potential given by (34), and to the right on to this embedding potential shifted by the potential step V_st, following (46).

The expansion coefficients in the basis set expansion of $\tilde{\eta}(z,t)$ in region I satisfy (53) and (55), with an extra term b_i added on to Γ_i (56) given by

$$b_i = \exp(-\mathrm{i}Et)\int_{z_l}^{z_r}\mathrm{d}z\,\chi_i(z)\delta V(z,t)\Psi(z). \tag{72}$$

As in the surface electric field calculation in section 4.2, we take $\delta t = 0.0025$ au in the time integration for accurate results.

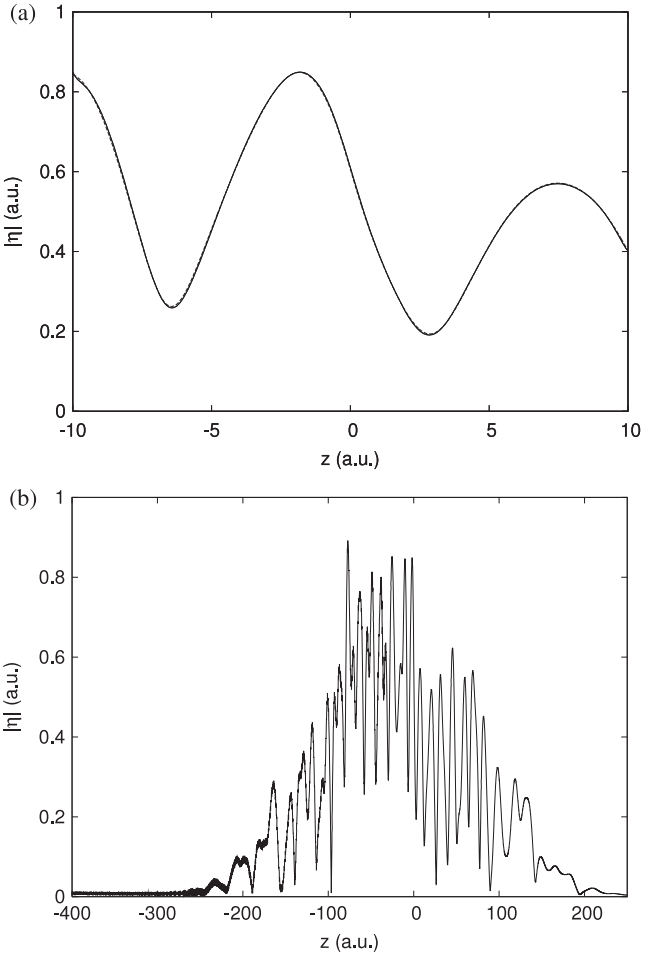

Figure 11. Excitation of a bulk state: magnitude of change in wavefunction at $t = 120$ au. (a) $|\tilde{\eta}|$ calculated using embedding with 25 basis functions, solid line; $|\tilde{\eta}|$ calculated over extended space using finite differences, dashed line. Plotted over embedding region between $z = -10$ au and 10 au. (b) $|\tilde{\eta}|$ from finite differences plotted over extended region.

We take a bulk state with energy $E = 0.3$ au and apply the time-dependent surface perturbation with frequency $\omega = 0.5$ au, starting at $t = 0$. The results for the modulus of the change in wavefunction at $t = 120$ au, calculated with 25 basis functions, are shown in figure 11(a), compared with results from a finite-difference calculation taken over the extended range $-1000 < z < 1000$ au. Figure 11(b) shows the finite-difference results over part of the extended range, and we see edge effects, propagating from the left-hand boundary and reaching $z = -100$ au. With the left-hand boundary in the finite-difference calculation at -1000 au, the results in the surface region become unusable beyond $t = 120$ au, a problem which of course does not affect embedding with its correct treatment of boundary conditions. We see from figure 11(a) that the embedding results are accurate, even with this relatively small basis set.

It is interesting to calculate the current in this case, not only as a sensitive test of the accuracy of the calculation, but also to illustrate the physics. Of course we must use

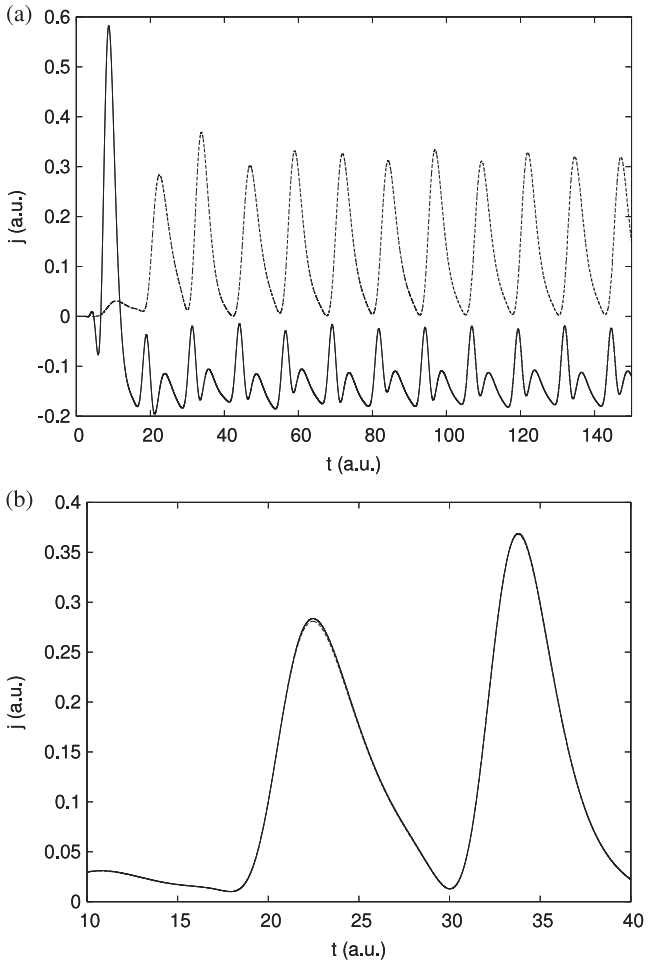

Figure 12. Excitation of a bulk state: current across boundaries of region I as a function of time. Positive current corresponds to charge *leaving* region I. (a) j calculated with embedding: solid line, across left-hand boundary at z_l; dashed line, across right-hand boundary at z_r. (b) Comparison of j at z_r using embedding (solid line), with finite differences (dashed line).

the full wavefunction given by (64) in the expression (63) for the current. Checking the accuracy first, we see from figure 12(b) that embedding works well. It is figure 12(a) which has physical content, and we see that after a short period of transient behaviour, the current entering the surface from the bulk (a negative current at z_l) and leaving the surface into vacuum (a positive current at z_r) both settle down to steady behaviour. In fact the currents balance out on average, as is shown by figure 13, giving the norm of $\tilde{\psi}(z,t)$ in the embedding region. We see that the charge in the surface region oscillates about a constant value, after a sudden loss of charge at about $t = 10$ au.

The results shown in figure 12(a) are in some ways surprising—we are solving the Schrödinger equation in the surface region with an embedding potential based on an outgoing Green function, and yet we are able to describe the current *entering* the surface from the bulk. This goes to show the power of Green function-based methods.

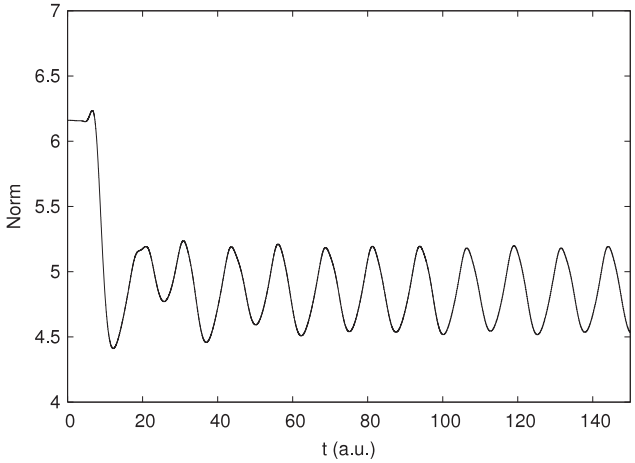

Figure 13. Norm of wavefunction in the embedding region as a function of time.

6. Conclusions

This embedding method provides the correct boundary conditions for solving the time-dependent Schrödinger equation in a limited region of space, region I, automatically matching the solution on to the time-evolving wavefunction in the rest of the system, region II. Once we have found the embedding kernel for region II, all that we have to do is to add this on to the Hamiltonian for region I and time-integrate the Schrödinger equation in this region. As we solve the time-dependent Schrödinger equation using the relatively small basis set needed to describe region I, this embedding method is very economical. In the examples in this paper we use a plane-wave basis to expand the wavefunction in region I, but any other basis set (see, for example, [31]) could be used.

The next stage in this project is to improve the numerical time-integration scheme, and then apply it to more realistic surface models to study surface electron excitation.

Acknowledgments

The author would like to thank Hiroshi Ishida, Pedro Echenique, and Txema Pitarke for their hospitality. It was during stays at their institutions that most of this work was carried out.

References

[1] Agostini P and DiMauro L F 2004 *Rep. Prog. Phys.* **67** 813–55
[2] Kienberger R, Goulielmakis E, Uiberacker M, Baltuska A, Yakovlev V, Bammer F, Scrinzi A, Westerwalbesloh Th, Kleineberg U, Heinzmann U, Drescher M and Krausz F 2004 *Nature* **427** 817–21
[3] van der Hart H W, Lysaght M A and Burke P G 2007 *Phys. Rev.* A **76** 043405
[4] Blanchet V, Zgierski M Z and Stolow A 2001 *J. Chem. Phys.* **114** 1194–205
[5] Miaja-Avila L, Lei C, Aeschlimann M, Gland J L, Murnane M M, Kapteyn H C and Saathoff G 2006 *Phys. Rev. Lett.* **97** 113604

[6] Cavalieri A L, Müller N, Uphes Th, Yakovlev V, Baltuška A, Horvath B, Schmidt B, Blümel L, Holzwarth R, Hendel S, Drescher M, Kleineberg U, Echenique P M, Kienberger R, Krausz F and Heinzmann U 2007 *Nature* **449** 1029–32
[7] Kulander K C, Schafer K J and Krause J L 1991 *Phys. Rev. Lett.* **66** 2601–4
[8] Boucke K, Schmitz H and Kull H-J 1997 *Phys. Rev.* A **56** 763–71
[9] McCurdy C W, Stroud C K and Wisinski M K 1991 *Phys. Rev.* A **43** 5980–90
[10] Piraux B and Shakeshaft R 1994 *Phys. Rev.* A **49** 3903–8
[11] Purvis J, Dörr M, Terao-Dunseath M, Joachain C J, Burke P G and Noble C J 1993 *Phys. Rev. Lett.* **71** 3943–6
[12] Hellums J R and Frensley W R 1994 *Phys. Rev.* B **49** 2904–6
[13] Inglesfield J E 1981 *J. Phys. C: Solid State Phys.* **14** 3795–806
[14] Inglesfield J E 2001 *Comput. Phys. Commun.* **137** 89–107
[15] Ishida H 2001 *Phys. Rev.* B **63** 165409
[16] Kemp R and Inglesfield J E 2002 *Phys. Rev.* B **65** 115103
[17] Isakov V 1998 *Inverse Problems for Partial Differential Equations* (New York: Springer)
[18] Ehrhardt M 1999 *VLSI Des.* **9** 325–38
[19] Moyer C A 2004 *Am. J. Phys.* **72** 351–8
[20] Kurth S, Stefanucci G, Almbladh C-O, Rubio A and Gross E K U 2005 *Phys. Rev.* B **72** 035308
[21] Henneberger W C 1968 *Phys. Rev. Lett.* **21** 838–41
[22] Ermolaev A M, Puzynin I V, Selin A V and Vinitsky S I 1999 *Phys. Rev.* A **60** 4831–45
[23] Bagchi A 1974 *Phys. Rev.* B **10** 524–53
[24] Szmytkowski R and Bielski S 2004 *Phys. Rev.* A **70** 042103
[25] Abramowitz M and Stegun I A (ed) 1965 *Handbook of Mathematical Functions* (New York: Dover)
[26] Gil A, Segura J and Temme N M 2002 *ACM Trans. Math. Softw.* **28** 325–36
[27] Chulkov E V, Sarría I, Silkin V M, Pitarke J M and Echenique P M 1998 *Phys. Rev. Lett.* **80** 4947–50
[28] Ishida H and Liebsch A 1998 *Phys. Rev.* B **57** 12 558–63
[29] Press W H, Flannery B P, Teukolsky S A and Vetterling W T 1989 *Numerical Recipes* (Cambridge: Cambridge University Press)
[30] Thijssen J M 2007 *Computational Physics* 2nd edn (Cambridge: Cambridge University Press)
[31] Thijssen J M and Inglesfield J E 1995 *Phys. Rev.* B **51** 17988–91